



1 **Data-driven discovery of mechanisms underlying present and near-** 2 **future precipitation changes and variability in Brazil**

3 Márcia Talita A. Marques¹, Maria Luiza Kovalski¹, Gabriel M. P. Perez¹, Thomas C. M. Martin¹, Edson
4 L. S. Y. Barbosa¹, Pedro Augusto S. M. Ribeiro¹, Roilan H. Valdes²

5 ¹MeteoIA, São Paulo, Brazil

6 ²Engie Brazil, São Paulo, Brazil

7 *Correspondence to:* Gabriel M. P. Perez (gabriel@meteoia.com)

8 **Abstract.** Untangling the complex network of physical processes driving regional precipitation regimes in the present (1979-
9 2014) and near-future climates (2020-2050) is fundamental to support a more robust scientific basis for decision making in
10 the water-energy-food nexus. We propose a data-driven mechanistic approach to: (Goal 1) identify changes and variability of
11 the regional precipitation mechanisms and (Goal 2) reduce the ensemble spread of future projections by weighting and
12 filtering models that satisfactorily represent these drivers in present climate. Goal 1 is achieved by applying the Partial Least
13 Squares (PLS) technique, a two-sided variant of principal component analysis (PCA), on a reanalysis dataset and 30
14 simulations of the future climate submitted to CMIP6 to discover the links between global sea-surface temperature (SST)
15 and precipitation in Brazil. Goal 2 is achieved by selecting and weighting the future climate simulations from climate models
16 that better represent the dominant modes discovered by the PLS in the present climate; with this subset of climate simulation,
17 we produce precipitation change maps following IPCC's WG1 methodology. The main mechanistic link discovered by the
18 technique is that the generalised warming of the oceans promotes a suppression of precipitation in Northeast and Southeast
19 Brazil, possibly mediated by the intensification of the Hadley circulation. We show that this pattern of precipitation
20 suppression is stronger in the near-future precipitation change maps produced using our methodology. This demonstrates that
21 a reduction of epistemic uncertainty is achieved after we select models that skillfully represent these mechanisms in the
22 present climate. Therefore, the approach is capable of supporting both a quantitative analysis of regional changes as well as
23 the construction of storylines supported by mechanistic evidence.

24 **1 Introduction**

25 Information about near-future regional precipitation change is crucial for planning and managing critical infrastructure, such
26 as hydropower plants, water reservoirs, and city planning. Unpreparedness for changes and variations in regional
27 precipitation regimes may lead to disruption in the water-food-energy supply chains as well as avoidable deaths and damages
28 by flooding and landslides. Although there is a degree of certainty about global precipitation changes (Shepherd et al., 2018),



29 such as the intensification of the hydrological cycle, a current major challenge in climate change science is informing
30 planners and decision-makers about regional changes within the critical time-frame of the next three decades.

31 Within this time frame, the two main sources of uncertainty in regional precipitation changes are model uncertainty and
32 internal variability (Hawkins and Sutton, 2011). Uncertainty due to the internal variability of the climate system is
33 impossible to reduce and is aleatoric and related to the chaotic nature of the system (Shepherd, 2019). Model uncertainty, on
34 the other hand, is epistemic in nature and stems from our limited knowledge of Earth's climate system and from the
35 challenges in translating this system into computer models. Currently, there are 131 available models on the CMIP6
36 database, each representing Earth's climate with a range of parameterizations and numerical modelling strategies.

37 In this study, we seek for a reduction of the epistemic uncertainty of regional precipitation changes in Brazil through a data-
38 driven process-based methodology of model selection and weighting. The method discovers the relationships between sea
39 surface temperature and precipitation in Brazil and evaluates the capability of CMIP6 models to reproduce these
40 precipitation mechanisms in the present climate. Later, the best models are selected and weighted to produce refined
41 precipitation maps. Due to the process-based nature of the method, it is also possible to isolate mechanisms and draw
42 storylines of plausible futures. The paper answers the following questions:

- 43 • What are the spatiotemporal links between global sea-surface temperature (SST) and regional precipitation change
44 and variability in Brazil?
- 45 • Many patterns have been identified in the literature, but here we choose to use a supervised ML approach to
46 systematically identify and quantify their importance
- 47 • Can we take advantage of these mechanisms to filter CMIP6 simulations and reduce the epistemic uncertainty of
48 regional precip changes?
- 49 • How precipitation will look like in the next 30 years in Brazil; as predicted by a filtered model ensemble, in which
50 we can consider the mean, the trend or individual model runs as possible futures.

51 **2 Materials & Methods**

52 **2.1 Data-driven discovery of precipitation mechanisms**

53 To discover the underlying mechanisms linking the SST spatiotemporal variability and regional precipitation in Brazil we
54 employ a data-driven dimensionality reduction method known as Partial Least Squares (PLS) adapted to a lat-lon grid; which
55 has been recently shown to successfully identify circulation mechanisms leading to precipitation (Perez et al, 2022).

56 The PLS method identifies pairs of latent variable vectors and that maximises the information present in XtY , where X and
57 Y represent two arrays of SST and precipitation, respectively; rows of X and Y represent the monthly averaged temporal
58 samples while the columns represent the spatial lat-lon grid points. The more familiar Principal Component Analysis (PCA)
59 can be seen as a special case where $X=Y$. The initial set, or mode, of latent variables is determined through the following
60 covariance Eq. (1):



61 $Cov(1,1) = \max \|u\| = \|v\| = 1 Cov(Xu, Yv),$ (1)

62 where u and v are temporally invariant arrays of loadings; in contrast to PCA, PLS yields a pair of loading matrices per
63 component rather than a single loading matrix; the first pair of loading matrices is the one in which the corresponding latent
64 vectors and are the most correlated. The following modes are found through repeating the process on the residuals of each
65 preceding pair.

66 The interpretation of PLS results should always consider scores and loadings concurrently. A positive loading correlation,
67 coupled with a positive trend in the scores, indicates an increase in signal strength over time. Conversely, when loadings
68 exhibit the same signal but are associated with a negative trend in scores, this suggests a decrease in signal intensity. A
69 detailed explanation of the method can be found in Wegelin (2000).

70 2.2 Present and future climate datasets

71 The PLS method was applied to two kinds of climate datasets: firstly, to present climate data from AMIP experiments and
72 reanalysis and, secondly, to the future climate simulations. In the AMIP experiments, atmospheric models are forced by
73 prescribed sea surface temperatures. The subsections below describe the methodologies and data behind the present and
74 future climate results.

75 2.2.1 Present climate (AMIP)

76 The first step was to establish a transfer function linking SST and precipitation month-to-month co-variability using the PLS
77 technique, for the reanalysis and atmosphere-only experiments. The goal is to identify models that accurately represent the
78 transfer function identified in the reanalysis in the present climate. To achieve this, we employ precipitation data derived
79 from the ERA5 reanalysis (Hersbach and Dee, 2016), in addition to precipitation data from 29 AMIP models from the
80 Coupled Model Intercomparison Project Phase 6 (CMIP6), as outlined in Table 1. Before the PLS technique was employed,
81 the ERA5 precipitation data underwent systematic error correction using observations from the Global Precipitation
82 Climatology Project (GPCP, Adler et al., 2018) as a reference through the quantile mapping method, which adjusts
83 probability distributions by individually matching each quantile to the respective quantile of the reference dataset (Jakob et
84 al., 2011). Each precipitation dataset was conservatively gridded to a regular $1^\circ \times 1^\circ$ lat-lon grid in a monthly temporal
85 resolution between 1979 and 2014. SST data was obtained from the COBE dataset, produced by the Japan Meteorological
86 Agency (Hiragana et al., 2014).

87 Table 1 - CMIP6 simulations, their native resolutions, vertical levels and source institutions

Model	Horizontal resolution	Vertical levels	Variant label	Institution
ACCESS-CM2	$1.875^\circ \times 1.25^\circ$	85	r1i1p1f1	CSIRO
ACCESS-ESM1-5	$1.875^\circ \times 1.25^\circ$	38	r1i1p1f1	CSIRO
BCC-CSM2-MR	$2.81^\circ \times 2.81^\circ$	46	r1i1p1f1	BCC



Model	Horizontal resolution	Vertical levels	Variant label	Institution
ACCESS-CM2	1.875° × 1.25°	85	r1i1p1f1	CSIRO
CAMS-CSM1-0	1° × 1°	31	r1i1p1f1	CAMS
CanESM5	2.81° × 2.81°	49	r1i1p1f1	CCCma
CESM2-WACCM	0.9° × 1.25°	70	r1i1p1f1	NCAR
CIESM	1° × 1°	30	r1i1p1f1	THU
CMCC-CM2-SR5	1° × 1°	30	r1i1p1f1	CMCC
CNRM-CM6-1	1.4° × 1.4°	91	r1i1p1f2	CNRM-CERFACS
CNRM-CM6-1-HR	1.4° × 1.4°	91	r1i1p1f2	CNRM-CERFACS
CNRM-ESM2-1	1.4° × 1.4°	91	r1i1p1f2	CNRM-CERFACS
EC-Earth3-CC	0.7° × 0.7°	91	r1i1p1f1	EC-Earth-Consortium
EC-Earth3-Veg	0.7° × 0.7°	91	r1i1p1f1	EC-Earth-Consortium
EC-Earth3-Veg-LR	1.1° × 1.1°	62	r1i1p1f1	EC-Earth-Consortium
FGOALS-f3-L	1° × 1°	32	r1i1p1f1	IAP/CAS
FGOALS-g3	2° × 2°	26	r1i1p1f1	IAP/CAS
GFDL-CM4	1° × 1°	33	r1i1p1f1	NOAA-GFDL
GFDL-ESM4	1° × 1°	49	r1i1p1f1	NOAA-GFDL
IITM-ESM	2° × 2°	64	r1i1p1f1	CCCR-IITM
INM-CM4-8	2° × 1.5°	21	r1i1p1f1	INM
INM-CM5-0	2° × 1.5°	73	r1i1p1f1	INM
IPSL-CM6A-LR	2.5° × 1.3°	79	r1i1p1f1	IPSL
KACE-1-0-G	1.9° × 1.3°	85	r1i1p1f1	NIMS-KMA
MIROC6	1.4° × 1.4°	81	r1i1p1f1	MIROC
MPI-ESM1-2-HR	0.93° × 0.93°	95	r1i1p1f1	MPI-M
MPI-ESM1-2-LR	1.9° × 1.9°	47	r1i1p1f1	MPI-M
MRI-ESM2-0	1.125° × 1.125°	80	r1i1p1f1	MRI
NESM3	1.9° × 1.9°	47	r1i1p1f1	NUIST
NorESM2-LM	2° × 2°	32	r1i1p1f1	NCC
TaiESM1	1.25° × 0.9°	30	r1i1p1f1	AS-RCEC

88

89 The models listed above, through their computational representations of the atmosphere, choices of parameterisation, vertical
 90 levels etc, provide unique numerical representations of the physical climate system. Each of these representations have a



91 distinct level of skill in simulating the mechanisms of precipitation variability and changes in Brazil. Therefore, we rank and
92 select the models with higher performance to represent the SST-precipitation transfer function revealed by the PLS analysis.
93 This ranking is based on the Normalised Root Mean Square Error (NRMSE), which is obtained by comparing the PLS scores
94 and loadings between each model and those derived from the ERA5 reanalysis. Models that exhibit $\text{NRMSE} < 0.6$ in at least
95 two out of the first four PLS components, are singled out as more reliably representing mechanisms that cause the
96 precipitation in Brazil while the rest is discarded for the remaining analysis.
97 After the model ranking and selection step, we provide a set of weights that will be later used for model averaging. This set
98 of weights is found by multiplying the inverse of the NRMSE by the importance of each PLS component; this is done so that
99 models that perform well in representing more relevant mechanisms are favoured during the model pooling step. The
100 importance of each PLS component is quantified by the coefficient of determination (r^2) of the reconstructed precipitation
101 using only that component and the original ERA5 precipitation.

102 **2.2.2 Future climate**

103 We employ the same PLS methodology on future climate simulations under the SSP2-2.45 scenario between 2020 and 2050;
104 in this near-future temporal range, we do not expect the choice of scenario to influence the results because scenario
105 uncertainty in regional precipitation changes only becomes relevant in later decades (Hawkins and Sutton, 2011).
106 Finally, the effectiveness of this methodology in reducing the uncertainty of near-future precipitation changes in the CMIP6
107 ensemble is assessed by comparing the uncertainty of all CMIP6 models listed in Table 1 with the uncertainty of the subset
108 of models selected by our methodology. The uncertainty of the climate change signal was computed for each grid cell by
109 determining the ratio (in %) between the ensemble mean climatologies of the SSP2-4.5 scenario for the years 2020-2050 and
110 the historical period of 1979-2014. To assess the robustness of the models, we apply the procedure adopted by the
111 Intergovernmental Panel on Climate Change (IPCC), as outlined in its Sixth Assessment Report, made available through the
112 Interactive Atlas developed by Working Group I (WGI). This approach determines the robustness of climate change signals
113 based on a strong model consensus, highlighting where at least 80% of the models agree on the sign of the predicted
114 changes.

115 **3 Results and discussion**

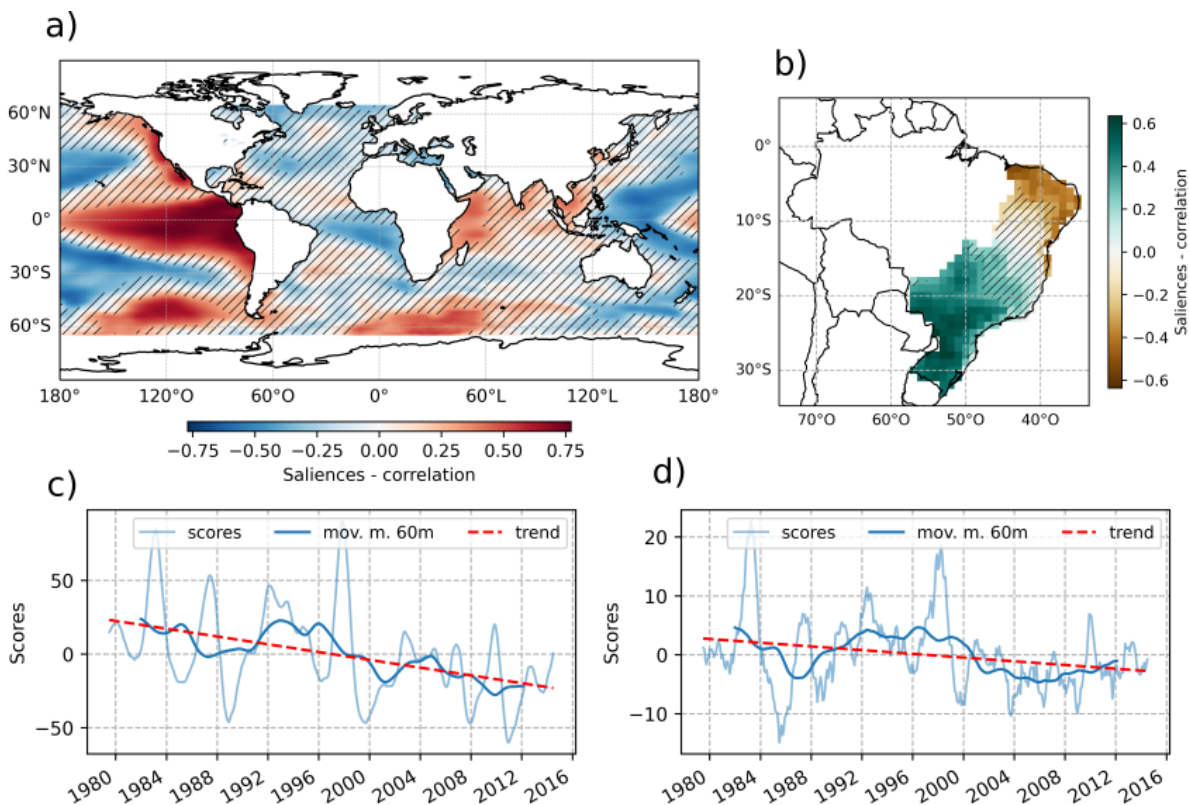
116 In this section, we present the results of the analysis for the present and future climates, discussing the underlying
117 precipitation mechanisms in reanalysis and model data. We also discuss the reduction of epistemic uncertainty of regional
118 precipitation changes obtained through the selection of models that skillfully represent precipitation mechanisms in the
119 present climate. In all results, the Legal Amazon area was cropped off; this is because precipitation in the Amazon region
120 presents significantly higher variability, dominating the results and washing out patterns in other areas that are also
121 socioeconomically relevant.



122 3.1 Precipitation mechanisms in the present climate (1979-2014)

123 In the present climate, the first PLS loadings matrix of the SST reveals a prominent positive pattern in the central Pacific
124 Ocean that aligns with the region dominated by the El Niño/Southern Oscillation (ENSO) phenomenon (Fig. 1a). This
125 ENSO-like pattern with high statistical significance (unhatched area) extends from the west coast of South America to the
126 Maritime Continent in the equatorial region, surrounded by a pattern of opposite signal. The associated PLS loadings matrix
127 for precipitation shows a significant positive correlation in South Brazil and a negative correlation in Northeast Brazil (Fig.
128 1b). The time series of the associated scores do not show a strong linear trend, reinforcing that this PLS mode is more
129 associated with a natural variability mechanism like ENSO than to climate change (Fig. 1d).

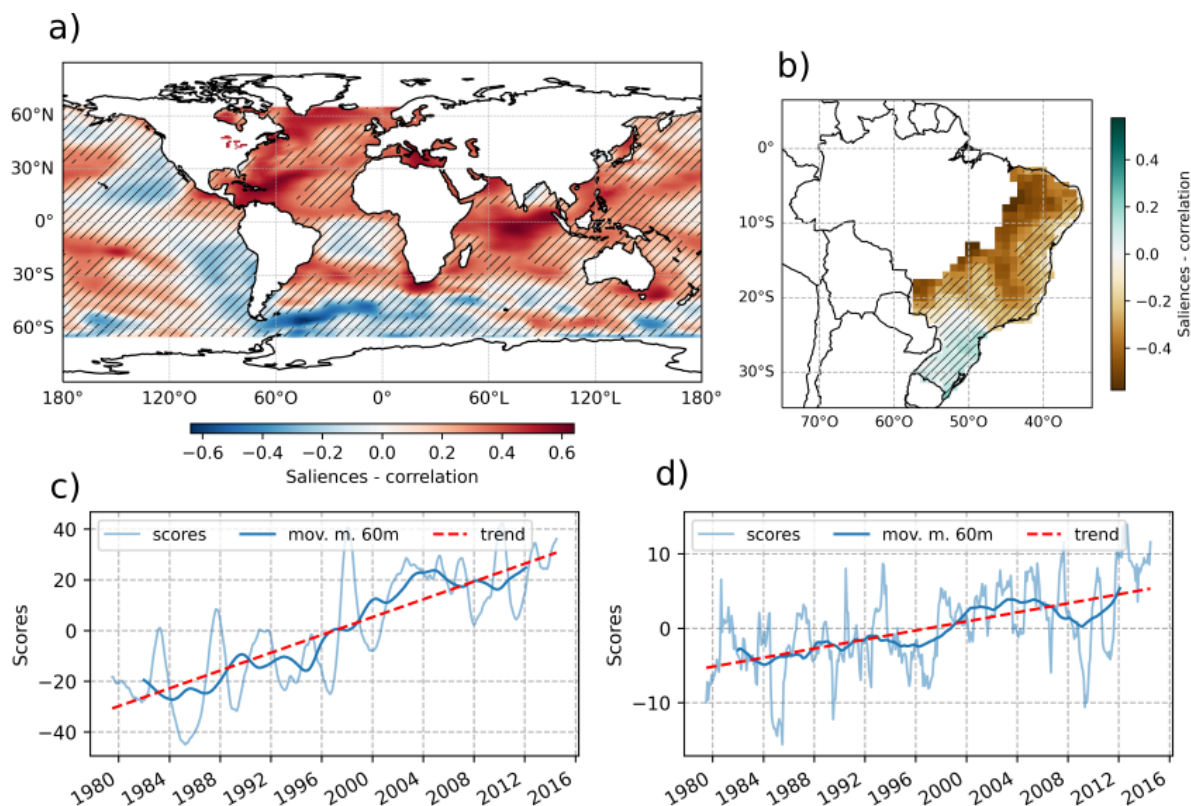
130 The global warming trend can explain the mostly positive SST loadings matrix and the increasingly positive scores time
131 series of the second PLS component (Fig. 2a,c). This warming oceanic pattern is linked to a precipitation reduction in most
132 of Southeast and Northeast Brazil (Fig. 2b,d). A possible explanation for this precipitation suppression is the expansion of
133 the Hadley cell under climate change (Lu et al., 2007; Grise & Davis, 2020) and, consequently, the restriction of the
134 equatorward motion of extratropical cyclones and their fronts, which are important precipitation mechanisms in Southeast
135 Brazil (Perez et al., 2021). Perez et al. (2022) has shown that a temporary intensification of the Hadley circulation during
136 positive NAO events leads to precipitation suppression in Southeast Brazil.



137



138 **Figure 1: First component of the PLS methodology applied using monthly precipitation data from ERA5 and SST data from**
 139 **COBE between 1979 and 2015. The spatial maps represent the loadings matrices and the time series represent the scores. The**
 140 **hatchings represent areas where the statistical confidence on the sign of the anomaly is lower than 95%.**



141 **Figure 2 - Second component of the PLS methodology applied using monthly precipitation data from ERA5 and SST data from**
 142 **COBE between 1979 and 2015. The spatial maps represent the loadings matrices and the time series represent the scores. The**
 143 **hatchings represent areas where the statistical confidence on the sign of the anomaly is lower than 95%.**
 144

145 Through the analysis of the PLS components in the present climate datasets, we are able to select and rank the models based
 146 on their performance to reproduce these components. The model selection is based on a threshold of $NRMSE < 0.6$, and the
 147 individual model weights are based on the inverse of the average NRMSE among the PLS components scaled by the
 148 importance of each component, as described in the Methodology section. The table below lists the selected models and their
 149 respective weights along with the components these models skillfully represent, later employed to construct the weighted
 150 ensemble mean in the future climate section.

151 Table 2 - List of selected models and their weights represented as a percentage of their contribution to the ensemble mean.

Model	Components	Weight (%)
CAMS-CSM1-0	1, 2, 4	7.76
CNRM-ESM2-1	1, 3, 4	7.73
GFDL-ESM4	2, 4	7.59



Model	Components	Weight (%)
BCC-CSM2-MR	1, 2, 4	7.37
EC-Earth3-CC	1, 2	7.11
EC-Earth3-Veg-LR	1, 2	7.08
EC-Earth3-Veg	2, 4	6.83
IPSL-CM6A-LR	2, 3, 4	6.69
KACE-1-0-G	1, 2	6.61
CNRM-CM6-1-HR	2, 3, 4	6.56
MPI-ESM1-2-HR	1, 4	6.28
CMCC-CM2-SR5	1, 2	6.19
FGOALS-f3-L	2, 3	6.18
MIROC6	1, 4	5.94
CESM2-WACCM	1, 4	4.08

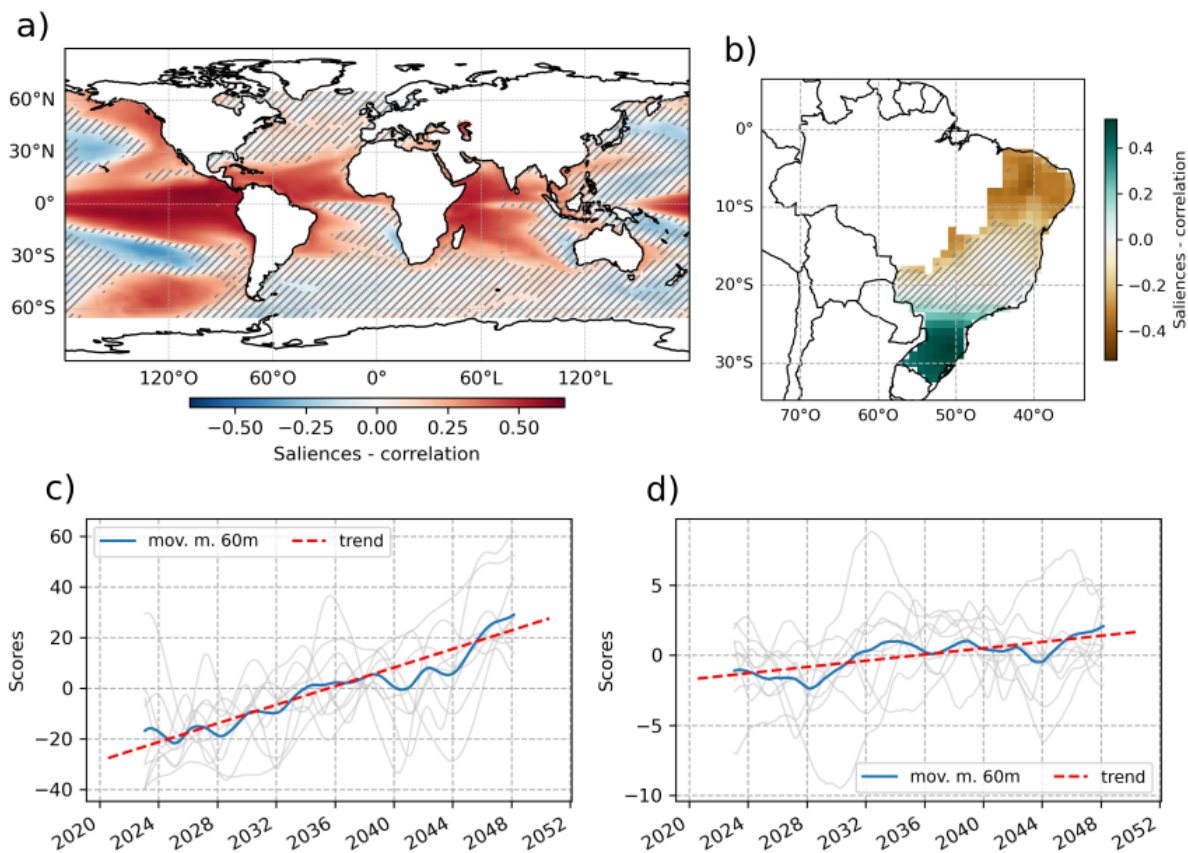
152

153 3.2 Precipitation mechanisms in the future climate (2020-2050)

154 The oceanic mechanisms driving precipitation in Brazil in the future climate (2020-2050) are discovered by applying the
155 PLS methodology in CMIP6 future climate simulations (Fig. 3 and 4). Figure 3 shows the first PLS component and Figure 4
156 the second PLS component; for each component, only models that performed well ($\text{NRMSE} < 0.6$) in the present climate are
157 considered. The spatial maps show the average loadings matrices of the model ensemble, where each model is weighed by
158 its skill in the present climate (Table 2); the hatched areas represent regions where at least 80% of the models disagree on the
159 sign of the loadings matrix.

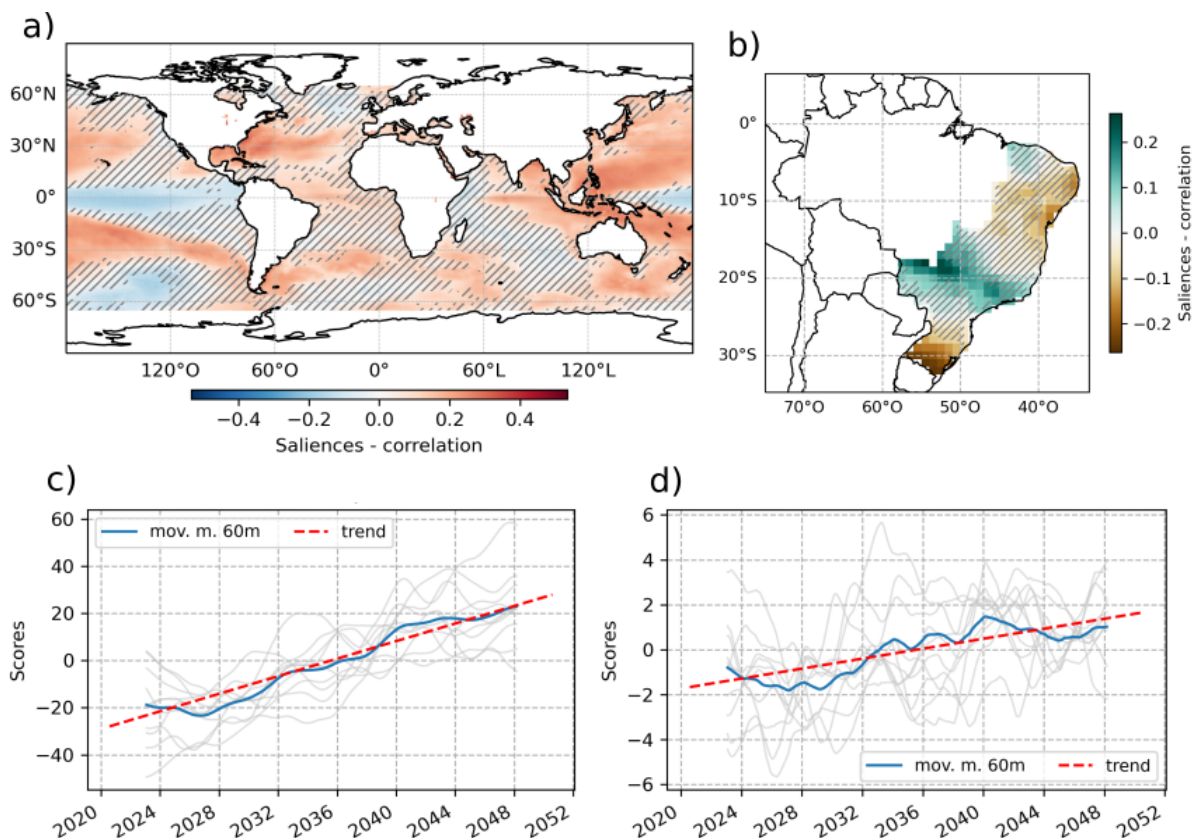
160 The first component shows a strong Niño-like pattern in the Central Pacific, similarly to what is found in the present climate
161 (Fig. 3a). However, unlike the present climate analysis, this Niño-like component shows a strong linear trend in the time
162 series of scores (Fig. 3c), suggesting that the climate models are mixing the natural variability of the ENSO phenomenon and
163 anthropogenic global warming; this warming trend can also be seen in the increasingly positive patterns in the tropical
164 Atlantic and Indian oceans. The impact of this warming trend in the Brazilian regional precipitation is a wetting pattern in
165 South Brazil and a drying pattern in Northeast Brazil, interfaced by a large region of uncertainty (Fig. 3b).

166 The second component illustrates a generalised warming trend in most regions of model agreement (Fig. 4a,c). This
167 component impacts precipitation in Brazil through a drying trend in the southernmost border of the country and a wetting
168 trend in the southeastern area. Some coastal areas in Northeast Brazil are significantly affected by a drying trend (Fig. 4b,d).



169
170
171
172
173

Figure 3 - First component of the PLS methodology applied using monthly precipitation data from CMIP6 models under the SSP2-4.5 scenario, listed in Table 2, between 2020 and 2050. The spatial maps represent the loadings matrices and the time series represent the scores. The regions with hatching indicate areas of uncertainty with < 80% agreement in the sign change among the models.



174
175 **Figure 4 - Second component of the PLS methodology applied using monthly precipitation data from CMIP6 models under the**
176 **SSP2-4.5 scenario, listed in Table 2, between 2020 and 2050. The spatial maps represent the loadings matrices and the time series**
177 **represent the scores. The regions with hatching indicate areas of uncertainty with < 80% agreement in the sign change among the**
178 **models.**

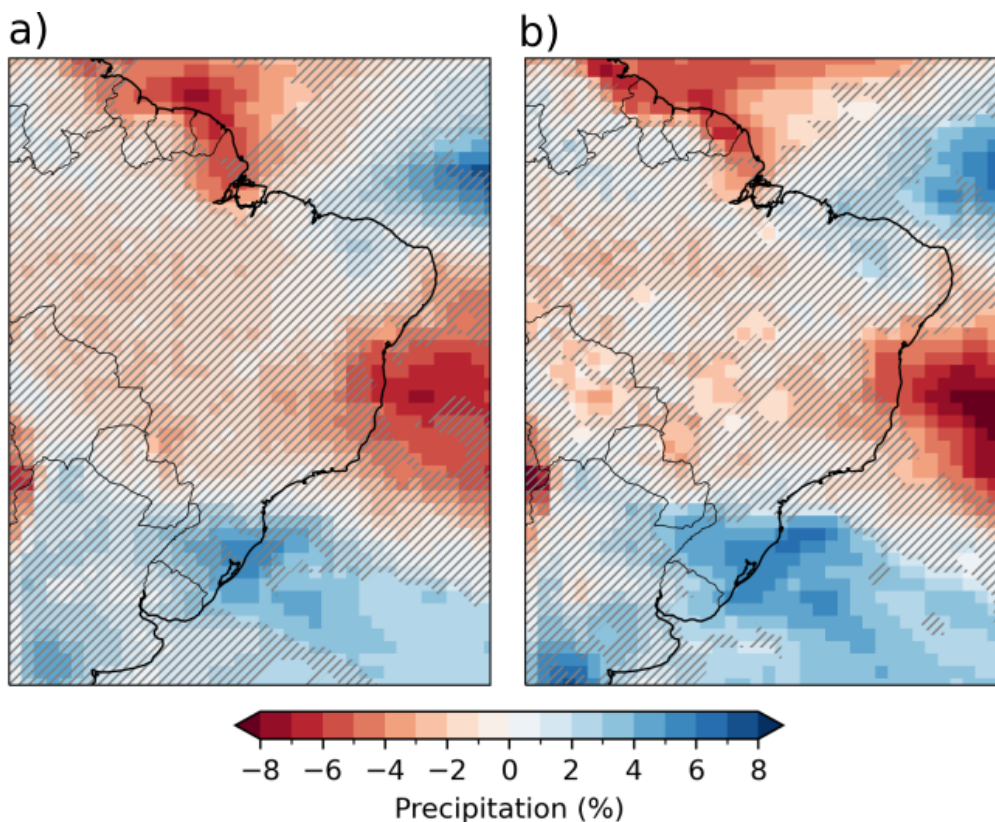
179 3.3 Future climate precipitation changes and uncertainty reduction

180 While the analysis of individual PLS components may support storyline approaches and mechanistic understanding, a
181 quantitative precipitation change map is often required by decision-making bodies. With that in mind, we provide an
182 uncertainty map based on the methodology employed by the IPCC in its 6th Assessment Report (Fig. 5). Here, we focus on
183 the percentage of projected changes in 2020-2050 relative to 1979-2014. The hatching highlights regions where there is a
184 significant lack of consensus, with at least 80% of the models analysed showing non-concordance, similar to the PLS
185 uncertainty maps shown in the previous section.

186 Figure 5a shows the future precipitation changes using all CMIP6 models, listed in Table 1, while Fig. 5b uses the subset of
187 models in Table 2 weighted by their skill in simulating precipitation mechanisms in the present climate (Fig. 5b). Firstly, we
188 notice that the reduction of epistemic uncertainty by the proposed methodology is revealed by stronger anomalies and fewer
189 hatched areas. Particularly, the South Atlantic Subtropical High (SASH) shows stronger negative anomalies, suggesting a
190 trend towards drier conditions in the region via an intensification of the Hadley cell descending branch. Moreover, the



191 positive changes in South Brazil have increased after the application of the methodology; this enhanced dipole between the
192 SASH and South Brazil is consistent with the mechanism of restriction of cold fronts revealed by the PLS in the present
193 climate and discussed in Sect. 3a. In other words, selecting and weighting models that reproduce important precipitation
194 mechanisms in the present climate has increased the clarity of what may happen in the region in the near-future climate.



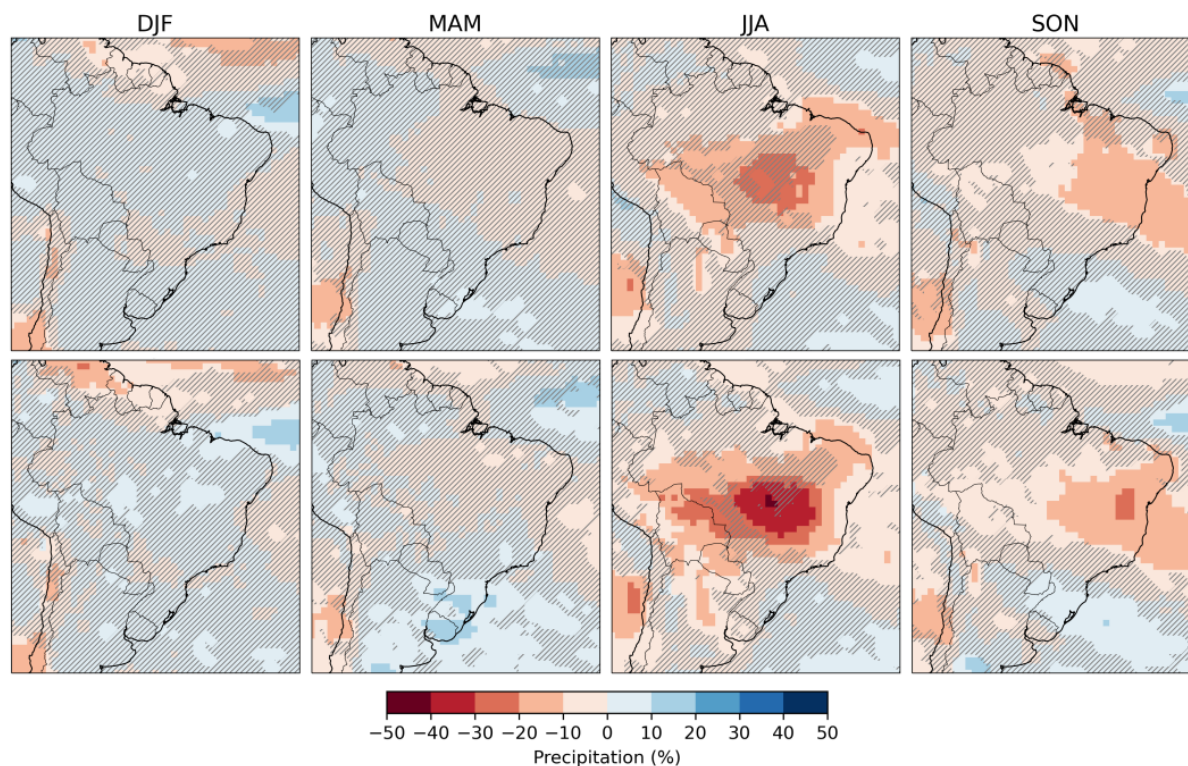
195
196 **Figure 5 - Percentual precipitation changes in 2020-2050 relative to 1979-2014 based on all assessed models, as listed in Table 1, (a)**
197 **and the percentual changes based on the selected models listed in Table 2 (b) from CMIP6 under the SSP2-4.5 scenario. The**
198 **regions with hatching indicate areas of uncertainty with < 80% agreement in the sign change among the models.**

199 Figure 6 shows the future precipitation changes broken down by season based on all models listed in Table 1 and only using
200 the models selected by the methodology (Table 2). A noticeable reduction of uncertainty across all seasons is evident when
201 comparing the hatched areas using all models versus only using the selected models, underscoring the success of our
202 process-based model selection methodology in enhancing our confidence in regional climate projections. The period from
203 December to May corresponds to the rainy season, characterised by a prevalence of uncertainties; this is in agreement with
204 Bazzanella et al. (2023) and Firpo et al. (2022), that also indicate that CMIP6 models perform better in the dry season than in
205 the wet season.

206 From June to November the Central and Northeast regions exhibit a clear drying pattern. In JJA, in particular, precipitation
207 in most of Brazil is largely driven by cold fronts, which, as previously discussed, can be restrained in higher latitudes if the



208 SASH is intensified. In SON, we expect an intensified SASH to also contribute to a later onset of the rainy season. This
209 drying pattern in JJA and SON is intensified in the subset of selected models. This is unsurprising, since the SASH
210 subsidence associated with an intensification of the Hadley circulation is one of the mechanisms discovered by the PLS
211 analysis in the present climate and used to select the best performing models.



212
213 **Figure 6 - Seasonal percentual precipitation changes in 2020-2050 relative to 1979-2014 based on all assessed models, as listed in**
214 **Table 1, (up) and the percentual changes based on the selected models listed in Table 2 (down) from CMIP6 under the SSP2-4.5**
215 **scenario. The regions with hatching indicate areas of uncertainty with < 80% agreement in the sign change among the models.**

216 4 Summary and Conclusions

217 This study aims to reduce the epistemic uncertainty of regional precipitation changes in Brazil through a data-driven process-
218 based methodology of model selection and weighting. To achieve this, we first employ the methodology to discover the main
219 precipitation drivers in the present climate (1979-2014) in a reanalysis dataset (Sect. 3a), revealing that the El Niño and the
220 generalised warming of the oceans are linked to significant precipitation impacts in Brazil (Fig. 1 and 2). A distinct positive
221 linear trend in the global warming component is linked to a drying of most of Northeast and Southeast Brazil. We propose
222 that the linking mechanism between these SST and precipitation patterns is the intensification of the Hadley circulation and,
223 consequently, of the subsidence at the South Atlantic Subtropical High.



224 The same methodology is then applied to CMIP6 present-climate simulations (Table 1) to evaluate the capability of CMIP6
225 models to simulate these precipitation drivers, thus creating a process-based model selection and weighting approach to
226 underpin the future climate analysis. From a total of 30 models, we select 15 models that are capable of simulating at least
227 two (Table 2) of the main regional precipitation drivers.

228 The mechanism discovery methodology is then applied to the near-future (2020-2050) climate simulations of the selected
229 models. We find that an ENSO-like pattern, tied to a generalised warming of the tropical oceans, is linked to an increase of
230 precipitation in South Brazil and a decrease in Northeast Brazil (Fig. 3 and 4), consistently with the present-climate
231 indication of an intensification of the Hadley circulation. This mechanistic view of regional precipitation changes can
232 underpin the development of storylines in future studies to support decision-making bodies in the water-energy-food nexus.

233 We go further to provide a quantitative view of regional precipitation changes based on the IPCC WG1 approach,
234 contrasting the uncertainty of precipitation changes using 30 CMIP6 models versus using the 15 selected models. We show
235 that the approach increased model agreement, particularly in South Brazil and SASH region. In the next 30 years (Fig. 6), a
236 noticeable reduction in uncertainty across all seasons is evident mostly from June to November. This period is characterised
237 by a clear drying pattern due to the strengthening of SASH, intensified within the subset of selected models, which leads to a
238 suppression of precipitation in Northeast and Southeast Brazil, possibly delaying the rainy season in these regions.

239 Our methodology employs an approach focused on understanding the underlying precipitation drivers rather than simply
240 comparing CMIP6 model precipitation with observations. By selecting and weighting models mechanistically, we achieve a
241 reduction of the epistemic uncertainty of the CMIP6 ensemble. This approach, as highlighted by Shepherd (2014), is a more
242 appropriate way to address the uncertainties of regional precipitation changes and to support physically sound storylines
243 regarding shifts in precipitation patterns.

244 **Acknowledgments**

245 This research results from the R&D project developed by MeteoIA for Engie Brazil, funded by ANEEL under Project No.
246 PD-00403-0054/2022.

247 **References**

- 248 Adler, R. et al.: The Global Precipitation Climatology Project (GPCP) Monthly Analysis (New Version 2.3) and a Review of
249 2017 Global Precipitation, *Atmosphere*, 9, 138, doi: <http://dx.doi.org/10.3390/atmos9040138>, 2018
- 250 Bazzanella, A.C. et al.: Performance of CMIP6 models over South America, *Clim. Dyn.*, doi:
251 <https://doi.org/10.1007/s00382-023-06979-1>, 2023.
- 252 Dias, C.G., Reboita, M.S. Assessment of CMIP6 Simulations over Tropical South America. *Revista Brasileira de Geografia*
253 *Física*, 14(3), 1282-1295, doi: <https://doi.org/10.26848/rbgf.v14.3.p1282-1295>, 2021.



- 254 Durkee, J. D., and Mote, T. L.: A climatology of warm-season mesoscale convective complexes in subtropical South
255 America, *Int. J. Climatol.*, doi:10.1002/joc.1961, 2009
- 256 Firpo, M. A. F. et al: Assessment of CMIP6 models' performance in simulating present-day climate in Brazil, *Frontiers in*
257 *Climate*, 4, doi: <https://doi.org/10.3389/fclim.2022.948499>, 2022.
- 258 Grise, K. M. and Davis, S. M.: Hadley cell expansion in CMIP6 models, *Atmos. Chem. Phys.*, 20, 5249–5268,
259 <https://doi.org/10.5194/acp-20-5249-2020>, 2020.
- 260 Gutiérrez, J. M., et al.: Atlas. In *Climate Change 2021: The Physical Science Basis. Contribution of Working Group I to the*
261 *Sixth Assessment Report of the Intergovernmental Panel on Climate Change* [Masson-Delmotte, V., P. Zhai, A. Pirani, S.L.
262 Connors, C. Péan, S. Berger, N. Caud, Y. Chen, L. Goldfarb, M.I. Gomis, M. Huang, K. Leitzell, E. Lonnoy, J.B.R.
263 Matthews, T.K. Maycock, T. Waterfield, O. Yelekçi, R. Yu, and B. Zhou (eds.)]. Cambridge University Press. In Press.
264 Interactive Atlas available from <http://interactive-atlas.ipcc.ch/>, 2021.
- 265 Hawkins, E., and Sutton, R. The potential to narrow uncertainty in projections of regional precipitation change, *Clim Dyn*,
266 37, 407–418, doi: <https://doi.org/10.1007/s00382-010-0810-6>, 2011.
- 267 Hersbach, H., and Dee D. ERA5 reanalysis is in production. *ECMWF Newsletter* 147:7, 2016.
- 268 Hirahara, S., M. Ishii, and Y. Fukuda: Centennial-Scale Sea Surface Temperature Analysis and Its Uncertainty. *J. Climate*,
269 27, 57–75, doi: <https://doi.org/10.1175/JCLI-D-12-00837.1>, 2014.
- 270 Themeßl, M. J., Gobiet, A., and Leuprecht, A.: Empirical-statistical downscaling and error correction of daily precipitation
271 from regional climate models, *Int J Climatol*, 31, 1530–1544. doi: 10.1002/joc.2168, 2011.
- 272 Lu, J., Vecchi, G. A., and Reichler T. : Expansion of the Hadley cell under global warming, *Geophys. Res. Lett.*, 34,
273 L06805, doi:10.1029/2006GL028443, 2007.
- 274 Perez, G. M. P., et al.: Atmospheric convergence zones stemming from large-scale mixing, *Weather Clim. Dynam.*, 2, 475–
275 488, doi: <https://doi.org/10.5194/wcd-2-475-2021>, 2021.
- 276 Perez, G. M. P., et al: Using a Synoptic-Scale Mixing Diagnostic to Explain Global Precipitation Variability from Weekly to
277 Interannual Time Scales. *J. Climate*, 35, 8225–8243, doi: <https://doi.org/10.1175/JCLI-D-22-0110.1>, 2022.
- 278 Shepherd, T. G.: Atmospheric circulation as a source of uncertainty in climate change projections. *Nature Geosci* 7, 703–
279 708, doi: <https://doi.org/10.1038/ngeo2253>, 2014.
- 280 Shepherd, T. G.: Storyline approach to the construction of regional climate change information, *Proc. R. Soc. A*, 475:
281 20190013. doi: <http://doi.org/10.1098/rspa.2019.0013>, 2019.
- 282 Shepherd, T. G., et al.: Storylines: an alternative approach to representing uncertainty in physical aspects of climate change,
283 *Climatic Change*, 151, 555–571, doi: <https://doi.org/10.1007/s10584-018-2317-9>, 2018.
- 284 Wegelin, J. A.: *A Survey of Partial Least Squares (PLS) Methods, with Emphasis on the Two-Blok Case*, Rel. téc. Seattle:
285 University of Washington, 2000.